Physical materials technology

Original article
UDC 537.6:548.73:538.91
DOI: https://doi.org/10.18721/JPM.19111

ELECTRONIC AND MAGNETIC PROPERTIES OF HAUSMANNITE

O. K. Kuvandikov, Z. M. Shodiev, J. Sh. Akhtamov ✉
Samarkand State University named after Sharof Rashidof,
Samarkand, Republic of Uzbekistan
✉ texnalogiya11@gmail.com

Abstract. In this work, the magnetic and electronic properties of the mineral hausmannite (Mn_3O_4) have been studied using both experimental and theoretical methods. Magnetic susceptibility χ was measured in the paramagnetic region over the temperature range of 288–1000 K using the Faraday method. The anomalies recorded at 657 K and 898 K in the $\chi^{-1}(T)$ plots were attributed to the Jahn–Teller effect, and this phenomenon was also found in the differential scanning calorimetry (DSC) analysis. Using the first-principles calculations based on the DFT+U method within the Quantum ESPRESSO package, the magnetic moment values of −4.1113 and 3.4801 Bohr magnetons (μ_B) for Mn^{2+} and Mn^{3+} ions, respectively, were obtained. The result of a net magnetization of 6.00 μ_B per cell was established which indicated the ferrimagnetic nature of the object. Band structure analysis confirmed the semiconductor nature of hausmannite (a theoretical band gap $E_g \approx 0{,}82$ eV).

Keywords: hausmannite, magnetic susceptibility, DSC, Curie – Weiss law, Jahn – Teller effect

For citation: Kuvandikov O. K., Shodiev Z. M., Akhtamov J. Sh., Electronic and magnetic properties of hausmannite, St. Petersburg State Polytechnical University Journal. Physics and Mathematics. 19 (1) (2026) 133–143. DOI: https://doi.org/10.18721/JPM.19111

Научная статья
УДК 537.6:548.73:538.91
DOI: https://doi.org/10.18721/JPM.19111

ЭЛЕКТРОННЫЕ И МАГНИТНЫЕ СВОЙСТВА ГАУСМАННИТА

О. К. Кувандиков, З. М. Шодиев, Ж. Ш. Ахтамов ✉
Самаркандский государственный университет имени Шарофа Рашидова,
г. Самарканд, Республика Узбекистан
✉ texnalogiya11@gmail.com

Аннотация. Проведено комплексное исследование магнитных и электронных свойств минерала гаусманнита Mn_3O_4 с применением как экспериментальных, так и теоретических методов. Магнитная восприимчивость χ измерялась в парамагнитной области в диапазоне температур 288 – 1000 K методом Фарадея. Аномалии, зарегистрированные на температурной зависимости $\chi^{-1}(T)$ при 657 и 898 K, интерпретированы как проявление эффекта Яна – Теллера; данное явление также обнаружено в ходе анализа методом дифференциальной сканирующей калориметрии (DSC). Расчеты из первых принципов в рамках теории функционала плотности и модели Хаббарда (DFT + U), выполненные с использованием пакета Quantum ESPRESSO, показали, что магнитные моменты ионов Mn^{2+} и Mn^{3+} составляют −4,1113 и 3,4801 магнетонов Бора μ_B, соответственно, что приводит к суммарной намагниченности 6,00 μ_B на элементарную ячейку, что свидетельствует о ферримагнитной природе соединения. Анализ зонной структуры гаусманнита подтвердил его полупроводниковый характер (теоретическая ширина запрещенной зоны $E_g \approx 0{,}82$ эВ).

Ключевые слова: гаусманнит, магнитная восприимчивость, DSC, закон Кюри – Вейсса, эффект Яна – Теллера

Для цитирования: Кувандиков О. К., Шодиев З. М., Ахтамов Ж. Ш. Электронные и магнитные свойства гаусманнита // Научно-технические ведомости СПбГПУ. Физико-математические науки. 2026. Т. 19. № 1. С. 133–143. DOI: https://doi.org/10.18721/ JPM.19111

Introduction

In recent years, manganese and its oxide compounds have garnered significant scientific interest due to their potential applications in ion exchange, molecular adsorption, photocatalysis, and water purification processes [1 – 4]. Manganese oxides exist in multiple structural forms that affects their electrical conductivity, magnetic behavior, and other physical parameters. They exhibit various oxidation states, namely, +2, +3, and +4, resulting from the loss of electrons from the $3d^5$ and $4s^2$ orbitals of manganese atoms. Among the naturally occurring manganese oxides, hausmannite (Mn_3O_4) is one of the most stable phases [5, 6]. It belongs to the spinel group and crystallizes in the tetragonal structure with the $I4_1/amd$ space group. Although it is often written as Mn_3O_4 its spinel-type structure (AB_2O_4) is better represented by the formula $Mn^{2+}[Mn^{3+}]_2O_4$, in which the Mn^{3+} ions occupy octahedral sites, and Mn^{3+} ions occupy tetrahedral sites [7 – 9].

Hausmannite possesses a band gap and exhibits semiconducting behavior [10 – 12]. Being a mixed-valence mineral, hausmannite plays an active role in various environmentally significant processes in mining regions [13 – 15].

The present study aims to investigate the electronic and magnetic properties of hausmannite to address existing gaps in the modern understanding of this mineral.

The research consists of two parts: experimental measurements and computational simulation.

The experimental part includes measurements of the temperature-dependent magnetic susceptibility $\chi(T)$ using the Faraday method, which is known for its high precision and suitability for small sample quantities. In addition, the Differential Scanning Calorimetry (DSC) analysis was carried out.

The theoretical part employs the framework of density functional theory (DFT) to analyze the material's electronic and magnetic characteristics. DFT-based modeling not only broadens the scope of the study but also enhances the reliability of the experimental findings. Software packages such as Quantum ESPRESSO [16, 17] were used to implement DFT approaches and accurately model the electronic structure of hausmannite. These calculations enable the determination of the density of states (DOS) and band structure, which are critical for understanding the mineral's conductivity and other electronic properties.

Research technique

Experimental details. The temperature dependence of the magnetic susceptibility, $\chi(T)$, of the hausmannite mineral was measured using the Faraday method. The measurements were carried out in an inert helium atmosphere [18]. The experimental values of the magnetic susceptibility at various temperatures were determined using the following expression:

$$\chi = \chi_r \frac{m_r \left(U_{h+s} - U_h\right)}{m_s \left(U_{h+r} - U_h\right)}. \quad (1)$$

In this context, U_{h+s} represents the compensating voltage measured for the combined sample and holder, while U_{h+r} corresponds to the compensating voltage for the standard reference and holder. U_h denotes the voltage drop of the empty holder (made of alumina, Al_2O_3). The symbols m_r and m_s refer to the masses of the reference and the sample, respectively, and χ_r indicates the magnetic susceptibility of the reference material.

The Mohr's salt was selected as the reference compound in the experiment. The relative measurement uncertainty of the magnetic susceptibility in the setup did not exceed 3% [19].

Computational details. For strongly correlated electron systems, particularly those involving transition metals such as Mn, Fe, Co, and Ni, the use of the extended Density Functional Theory with Hubbard U (DFT+U) approach is considered appropriate. This method accounts for the Coulomb repulsion between localized electrons, thereby more accurately representing the band gap typically observed in semiconductors or dielectric materials.

The crystal lattice parameters required for the DFT + U calculations of hausmannite were obtained from the Materials Project database [20]. The DFT+U computations were performed in the ferrimagnetic (FiM) phase using the Quantum ESPRESSO software package. The Hubbard U parameters employed were as follows:

$$U(Mn) = 4 \text{ eV}, U(O) = 0 \text{ eV}.$$

A Monkhorst – Pack k-point mesh of 6×6×6 was adopted. The plane-wave energy cutoff for the wavefunctions was set to *ecutwfc* = 56.6484 Ry, while the energy cutoff for charge density and potentials was set to *ecutrho* = 701.654 Ry. All calculations utilized Kresse – Joubert PAW-type pseudopotentials.

Results and discussion

The magnetic susceptibility of hausmannite (Mn_3O_4) in the paramagnetic region was experimentally measured using the Faraday method over a temperature range of 288 – 1000 K. Hausmannite is known to exhibit ferrimagnetic behavior, with a transition from the ferrimagnetic state to paramagnetic one occurring at approximately 43.1 K. Specifically, R. A. Robie and B. S. Hemingway [21] investigated the low-temperature heat capacity of Mn_3O_4 over the range of 5 – 380 K using an adiabatically shielded calorimeter and identified the magnetic phase transition at 43.12 K. A closely matching value was later reported by K. Chhor et al. [22], who measured the heat capacity of Mn_3O_4 from 10 to 310 K using an automated adiabatic calorimeter and determined the magnetic transition temperature to be 43.15 K.

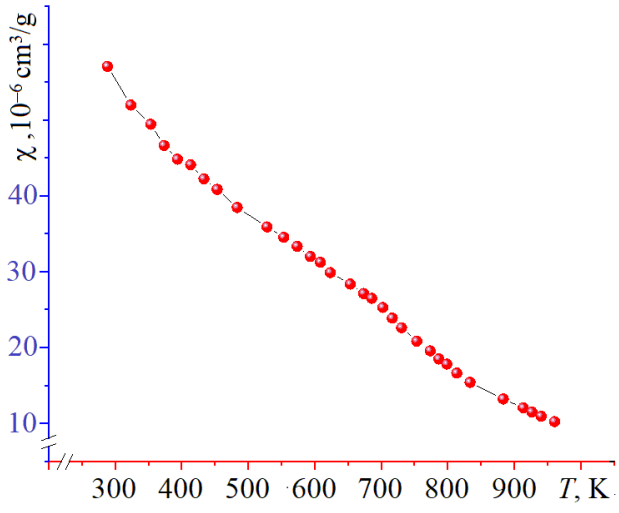

Fig. 1. A plot of the magnetic susceptibility versus temperature in the paramagnetic region for hausmannite Mn_3O_4

The temperature-dependent magnetic susceptibility $\chi(T)$ of hausmannite in the paramagnetic region is shown in Fig. 1. As can be seen in the plot, the magnetic susceptibility decreases monotonically with increasing temperature. This behavior is attributed to the disruption of the thermally ordered magnetic moments of Mn atoms under the influence of an external magnetic field, due to increasing thermal agitation.

Fig. 2, *a* shows the inverse magnetic susceptibility, i. e. $\chi^{-1}(T)$ curve for hausmannite, where distinct anomalies are observed at 657 K and 898 K. In order to scientifically interpret these anomalies and verify their thermal origin, we conducted a Differential Scanning Calorimetry (DSC) analysis of the sample (see Fig. 2, *b*). In the high-temperature region, a polymorphic phase transition from α-Mn_3O_4 to β-Mn_3O_4 was detected at 1449 K, where the structure transforms from a tetragonal spinel (α-phase) to a cubic one (β-phase). A similar transition was reported by K. T. Jacob et al. [23], who observed this transformation at approximately 1445 K.

The anomalies at 657 K and 898 K in the $\chi^{-1}(T)$ curve closely correspond to the endothermic peaks observed in the DSC plot at 662.3 K and 890.7 K, respectively, with only minor deviations. These transitions are attributed to Jahn –Teller distortions, which, as far as are known, affect the electronic structure and local symmetry of transition metal oxides such as Mn_3O_4.

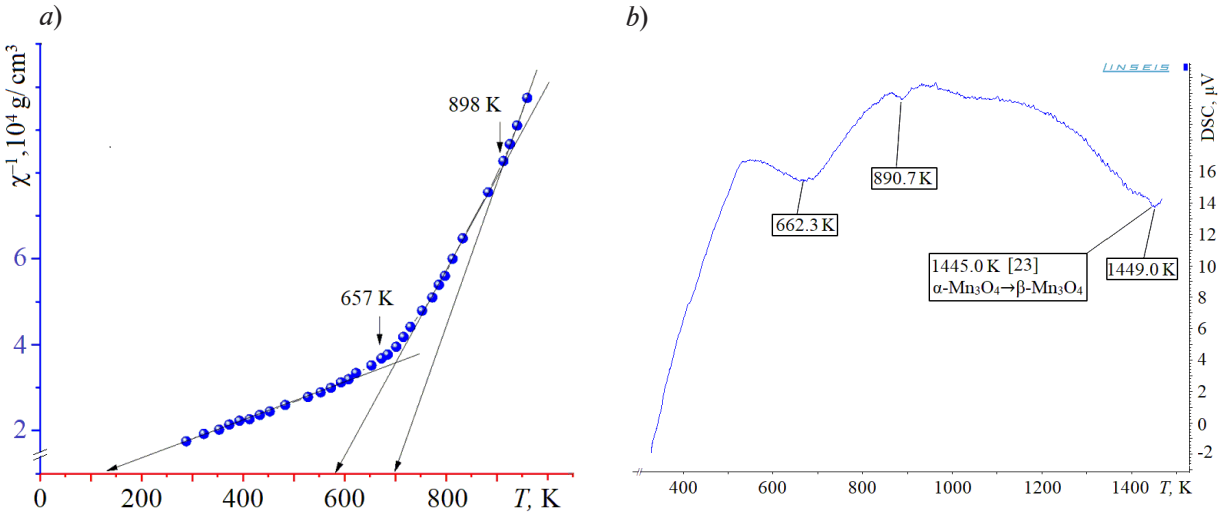

Fig. 2. The results of measuring the inverse magnetic susceptibility versus temperature of the sample (*a*) and its Differential Scanning Calorimetry (DSC) analysis (*b*)

In the Mn_3O_4 structure, Mn^{3+} ions occupy octahedral sites, and due to their d^4 electronic configuration $^3t_{2g}{}^1e_g$, they are highly susceptible to Jahn – Teller distortions. This phenomenon was discussed in detail by D. Jarosch [8], as illustrated in Fig. 3. According to his analysis, the Mn^{3+}– O^{2-} bond lengths in the octahedral coordination are divided into two distinct groups: four shorter bonds of approximately 1.930 Å and two longer bonds of ~2.282 Å. The deviation from perfect octahedral symmetry and the clear difference in bond lengths are strong indicators of Jahn – Teller distortion.

This effect alters the exchange interaction energy in the sample, which, in turn, affects its magnetic properties [24 – 26]. As temperature increases, the disparity between the Mn^{3+}– O^{2-} bond lengths also changes, leading to anomalies (kinks) in the $\chi^{-1}(T)$ magnetic susceptibility curve.

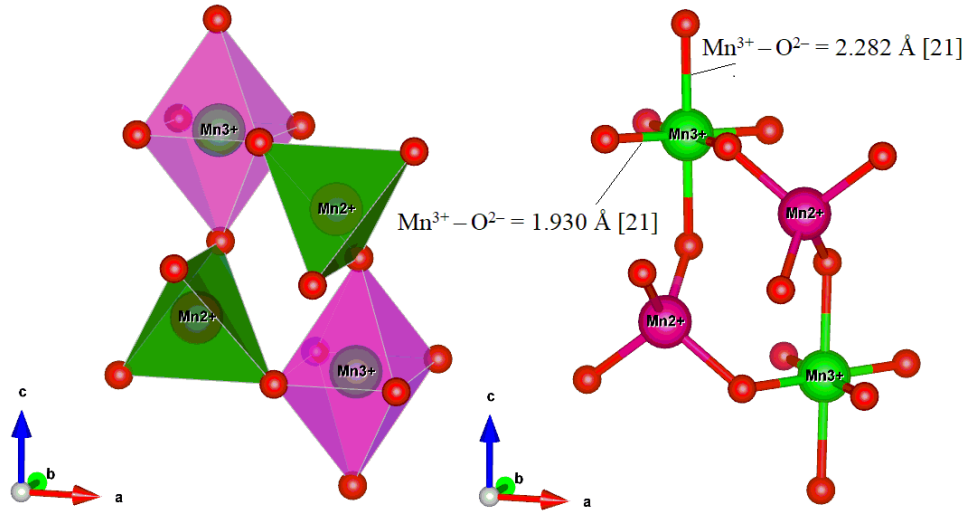

Fig. 3. Models of the crystal structure of hausmannite including oxygen octahedra and tetrahedrons; the Mn^{3+} ion is located in octahedral coordination, and this form experiences a strong Jahn – Teller distortion: the Mn^{3+}– O^{2-} bond lengths differ (see also the description in the text)

According to Fig. 2, *a*, the $\chi^{-1}(T)$ dependence consists of three linear regions, indicating that the variation of magnetic susceptibility in this range follows the Curie – Weiss law. In the first temperature interval of 653 – 288 K, the positive value of the Curie temperature θ_p (127 K) indicates ferrimagnetic ordering in hausmannite. In this region, the effective magnetic moment was determined to be $\mu_{eff} = 3\ \mu_B$, and the magnetic moment per formula unit was found to be $\mu_{for} = 5.2\ \mu B$. The values for the next intervals are presented in Table 1.

Table 1

Experimental results for the hausmannite (Mn_3O_4) sample calculated using the Curie – Weiss law from the $\chi^{-1}(T)$ plots (see Fig. 2, *a*)

Temperature interval, K	θ_p	C,10^{-4} cm^3·g^{-1}·K	μ_{eff}	μ_{for}
			μ_B	
288 – 653	127	206.0	3.0	5.20
753 – 913	577	45.85	1.4	2.46
913 – 960	698	31.86	1.2	2.00

Notations: θ_p is the paramagnetic Curie temperature, C is the Curie – Weiss constant, μ_{eff} is the effective magnetic moment, μ_{for} is the magnetic moment per formula unit (μ_B is the Bohr magneton).

The results of the DFT+U calculation. The electronic density of states (DOS) of Mn_3O_4 (hausmannite) obtained by using the DFT+U calculations is shown in Fig. 4. The DOS for $Mn^{2+}$and Mn^{3+} ions exhibits spin polarization around the Fermi level. The total densities of states for spin-up and spin-down configurations are asymmetric and differ significantly, indicating the presence of ferrimagnetic ordering. The $Mn^{2+}$and Mn^{3+} ions are aligned in opposite spin orientations, resulting in a net uncompensated magnetic moment. At the Fermi level ($E = 0$), the DOS is zero, confirming the semiconductor nature of hausmannite.

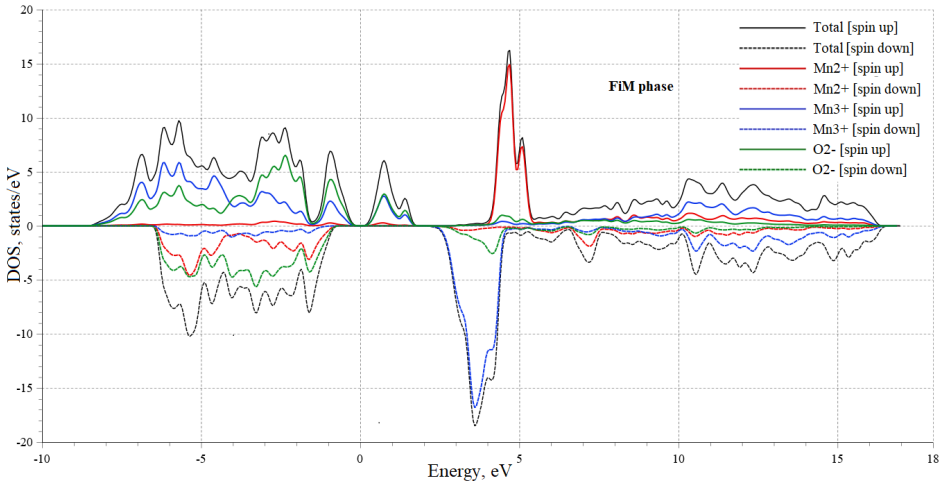

Fig. 4. Total and partial densities of states (DOS) of the hausmannite (Mn_3O_4) for spin-up and spin-down ion configurations

Table 2 presents the magnetic parameters of hausmannite. The magnetic moment of Mn^{2+} ion is −4.1113 μB, with the negative sign indicating antiferromagnetic alignment. The Mn^{3+} ion exhibits a magnetic moment of +3.4801 μ_B, and both values are in good agreement with the results reported by P. R. G. Gonçalves et al. [15]. The oxygen ion (O^{2-}) exhibits a magnetic moment of approximately −0.0718 μ_B, which is attributed to spin polarization arising from hybridization and superexchange interactions with neighboring Mn atoms. Due to the incomplete compensation of the antiparallel spins of Mn^{2+} and Mn^{3+} ions, a net magnetic moment of 6.00 μ_B per cell is produced. This value further confirms the ferrimagnetic nature of hausmannite.

Table 2

Results of DFT+U calculations for Mn_3O_4

Ion	Magnetic moment, μ_B	Magnetization, μ_B/cell	
		Total	Absolute
Mn^{2+}	–4.1113 (–4.3 [15])	6.00	26.84
Mn^{3+}	+3.4801(+3.5 [15])		
O^{2-}	–0.0718		

Fig. 5 presents the band structure of Mn_3O_4, where the blue (spin-up) and red (spin-down) bands are not symmetric. This asymmetry indicates that the magnetic moments in the material are not fully compensated and the net magnetization is non-zero. In the crystal structure of Mn_3O_4, both $Mn^{2+}$and Mn^{3+} ions are present, with their electron spin states oriented in opposite directions, resulting in ferrimagnetic behavior.

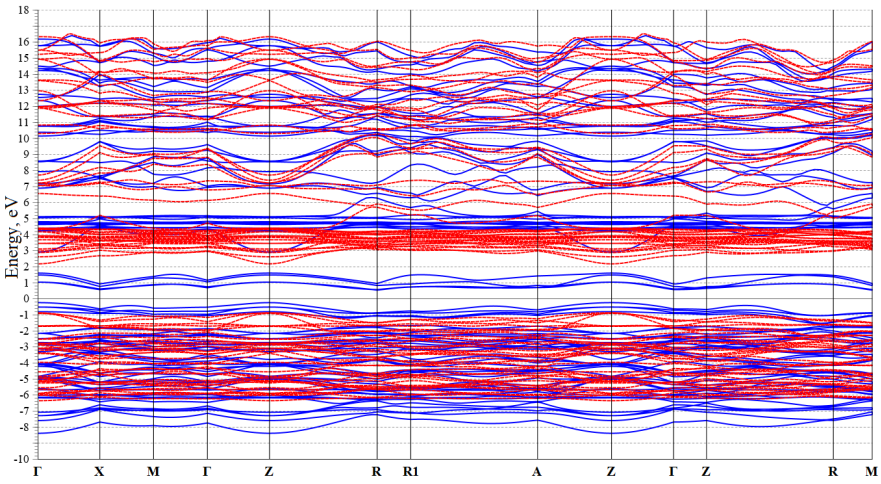

Fig 5. Band structure of Mn_3O_4

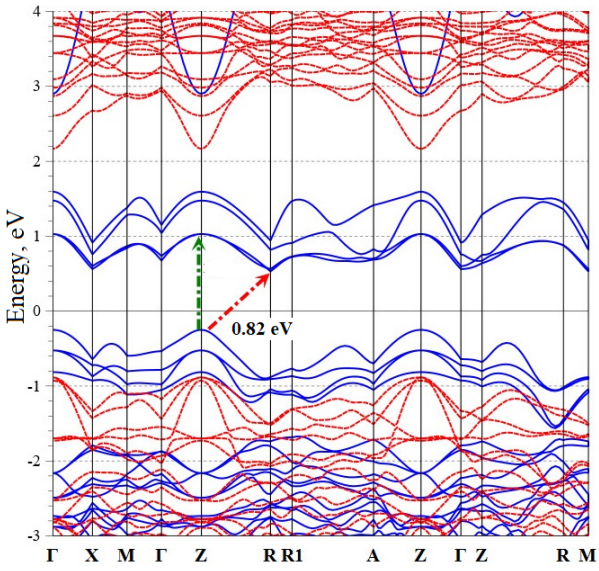

Fig. 6. Electronic band structure of Mn_3O_4 showing the energy states near the Fermi level

According to the band structure calculations of Mn_3O_4, an energy band gap of 0.82 eV (0.8 eV, as given in Ref. [15]) between the valence and conduction bands is observed, as shown in Fig. 6. Experimental studies report higher band gap values for Mn_3O_4: 2.07 eV for nanoparticles and 2.51 eV for thin films of this oxide [11, 12]. It is well known that the Generalized Gradient Approximation (GGA) functional used in our study tends to underestimate the band gap. When hybrid exchange-correlation functionals such as B3LYP, PBE0, and HSE are employed, the calculated band gap values for hausmannite are in much better agreement with experimental results [27 – 30]. However, since the primary focus of our study is on the magnetic properties, we limited our approach to GGA-level calculations.

ELF analysis. The Electron Localization Function (ELF) map serves as a powerful visual tool for analyzing the spatial distribution of electrons. It plays a crucial role in identifying regions of high electron localization, interatomic electron density distributions, and the nature of chemical bonding within the crystal structure [31].

Fig. 7, *a* shows the primitive crystal lattice of Mn_3O_4 where the electrons are strongly localized around the manganese ions. In contrast, the oxygen ions exhibit delocalized electron distribution, with the electron cloud extending toward the Mn–O bond centers. However, there is no evident hybridization between the oxygen orbitals and those of Mn, suggesting that ionic bonding is predominant in hausmannite.

Fig. 7, *b* illustrates the distribution of electron density relative to atomic centers in terms of ELF isosurfaces. No significant electron density relief is observed between Mn atoms, whereas various ELF reliefs are found between Mn and O atoms at different heights, indicating localized electron density in these bonding regions.

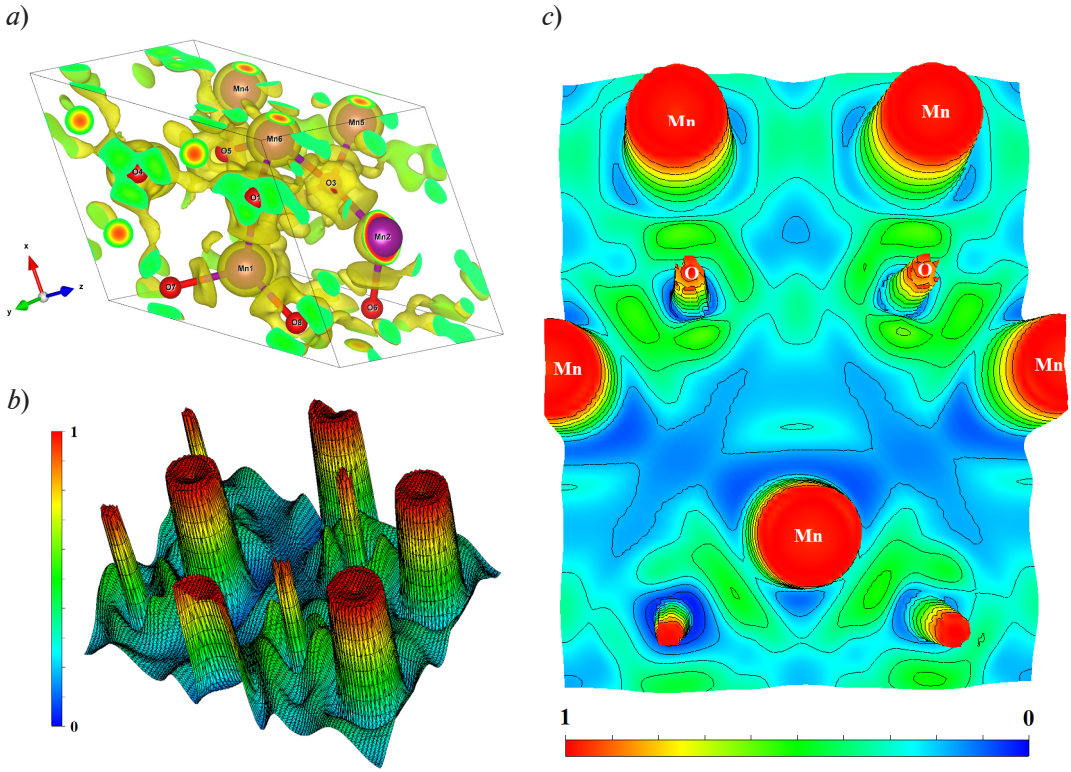

Fig. 7. ELF map of the Mn_3O_4 mineral including 3D views (*a*, *b*), and the 2D projection (*c*)

As shown in Fig. 7, *c*, the space Mn–Mn between atoms appears in blue, indicating the region of lowest electron density. This further confirms that bonding occurs predominantly through the oxygen atoms rather than direct Mn–Mn interaction.

Summary

In this study, the magnetic and electronic properties of the hausmannite (Mn_3O_4) mineral were investigated. In the paramagnetic phase, magnetic susceptibility $\chi(T)$, measured using the Faraday method, was found to decrease monotonically with increasing temperature. The $\chi^{-1}(T)$ plot exhibited anomalies at 657 K and 898 K, which were attributed to Jahn – Teller distortions. These distortions were further confirmed by endothermic effects observed using Differential Scanning Calorimetry (DSC) analysis at corresponding temperatures.

First-principles calculations based on the DFT+U approach revealed magnetic moments of −4.1113 μ_B for Mn^{2+} and +3.4801 μ_B for Mn^{3+} ions. The density of states (DOS) analysis confirmed a ferrimagnetic spin arrangement. Band structure calculations indicated that Mn_3O_4 exhibits semiconducting behavior with an estimated band gap of $E_g \approx 0.82$ eV. The analysis of Electron Localization Function (ELF) maps demonstrated ionic bonding characteristics in the Mn–O bonds.

REFERENCES

1. **Chen H., He J.,** Facile synthesis of monodisperse manganese oxide nanostructures and their application in water treatment, J. Phys. Chem. C. 112 (45) (2008) 17540–17545.

2. **Zhai Y., Zhai J., Zhou M., Dong S.,** Ordered magnetic core–manganese oxide shell nanostructures and their application in water treatment, J. Mater. Chem. 19 (38) (2009) 7030–7035.

3. **Chen H., Chu P. K., He J., et al.,** Porous magnetic manganese oxide nanostructures: synthesis and their application in water treatment, J. Colloid Interface Sci. 359 (1) (2011) 68–74.

4. **Imboon T., Khumphon J., Yotkuna K., et al.,** Enhancement of photocatalytic by Mn_3O_4 spinel ferrite decorated graphene oxide nanocomposites, SN Appl. Sci. 3 (22 May) (2021) 653.

5. **Grundy A. N., Hallstedt B., Gauckler L. J.,** Assessment of the Mn–O system, J. Phase Equilib. 24 (1) (2003) 21–39.

6. **Safarov R. Z., Baikenov Y. A., Zhandildenova A. K., et al.,** Phase transitions and structural evolution of manganese ores during high-temperature treatment, Metals. 15 (1) (2025) 89.

7. **Aminoff G.,** Über die Kristallstruktur von Hausmannit ($MnMn_2O_4$) [On the crystal structure of hausmannite ($MnMn_2O_4$)], Z. Kristallogr. Cryst. Mater. 64 (1) (1926) 475–490.

8. **Jarosch D.,** Crystal structure refinement and reflectance measurements of hausmannite, Mn_3O_4, Mineral. Petrol. 37 (1) (1987) 15–23.

9. **Baron V., Gutzmer J., Rundlöf H., Tellgren R.,** The influence of iron substitution on the magnetic properties of Hausmannite, $Mn^{2+}(Fe,Mn)^{3+}{}_2O_4$, Am. Mineral. 83 (7–8) (1998) 786–793.

10. **Hosny N. M., Dahshan A.,** Facile synthesis and optical band gap calculation of Mn_3O_4 nanoparticles, Mater. Chem. Phys. 37 (2) (2012) 637–643.

11. **Dubal D. P., Dhawale D. S., Salunkhe R. R., Fulari V. J., Lokhande C. D.** Chemical synthesis and characterization of Mn_3O_4 thin films for supercapacitor application, J. Alloys Compd. 497 (1–2) (2010) 166–170.

12. **Jha A., Thapa R., Chattopadhyay K. K.,** Structural transformation from Mn_3O_4 nanorods to nanoparticles and band gap tuning via Zn doping, Mater. Res. Bull. 47 (3) (2012) 813–819.

13. **Freitas E. T. F., Montoro L. A., Gasparon M., Ciminelli V. S. T.,** Natural attenuation of arsenic in the environment by immobilization in nanostructured hematite, Chemosphere. 138 (Nov) (2015) 340–347.

14. **Pulleri J. K., Singh S. K., Yearwar D., et al.,** Morphology dependent catalytic activity of Mn_3O_4 for complete oxidation of toluene and carbon monoxide, Catal. Lett. 151 (1) (2020) 172–183.

15. **Gonçalves P. R. G., De Abreu H. A., Duarte H. A.,** Stability, structural, and electronic properties of hausmannite (Mn_3O_4) surfaces and their interaction with water, J. Phys. Chem. C. 122 (36) (2018) 20841–20849.

16. **Giannozzi P., Baroni S., Bonini N., et al.,** QUANTUM ESPRESSO: a modular and open-source software project for quantum simulations of materials, J. Phys.: Condens. Matter. 21 (39) (2009) 395502.

17. **Davletshina A. D., Yakshibaev R. A., Bickulova N. N.,** The band structure of solid solutions of copper and silver chalcogenides, St. Petersburg State Polytechnic University Journal. Physics and Mathematics. (2 (170)) (2013) 33–38 (in Russian).

18. **Kuvandikov O. K., Shodiev Z. M., Khasanov Kh. B., et al.,** Ferrimagnetic properties of the $FeCr_2O_4$ chromite and $TiFe_2O_4$ titanomagnetite minerals at high temperatures, Metallofiz. Noveishie Tekhnol. 47 (6) (2025) 595–600.

19. **Kuvandikov O., Shodiev Z., Usarov U., et al.,** Paramagnetic properties of the rock minerals pyrrhotite and pentlandite at high temperatures, AIP Conf. Proc. 3304 (1) (2025) 020009.

20. **Persson K.,** Lawrence Berkeley National Laboratory and US. Department of Energy. Office of Scientific and Technical Information. Materials data on Mn_3O_4 (SG:141) by Materials Project, Materials Project, 2014. URL: https://doi.org/10.17188/1183671.

21. **Robie R. A., Hemingway B. S.,** Low-temperature molar heat capacities and entropies of MnO_2 (pyrolusite), Mn_3O_4 (hausmanite), and Mn_2O_3 (bixbyite), J. Chem. Thermodyn. 17 (2) (1985) 165–181.

22. **Chhor K., Bocquet J. F., Pommier C., Chardon B.,** Heat capacity and thermodynamic behaviour of Mn_3O_4 and $ZnMn_2O_4$ at low temperatures, J. Chem. Thermodyn. 18 (1) (1986) 89–99.

23. **Jacob K. T., Kumar A., Rajitha G., Waseda Y.,** Thermodynamic data for Mn_3O_4, Mn_2O_3 and MnO_2, High Temp. Mater. Process. 30 (4) (2011) 459–472.

24. **Duan J., Huang M., Song M., et al.,** Suppressing Jahn–Teller distortion in manganese oxides for high-performance aqueous zinc-ion batteries, Materials. 18 (12) (2025) 2817.

25. **Yu X., Qian K., Du L., et al.,** A strong Jahn − Teller distortion in Mn_3O_4–MnO heterointerfaces for enhanced silver catalyzed formaldehyde reforming into hydrogen, Sustain. Energ. Fuels. 6 (12) (2022) 3068–3077.

26. **Kuvandikov O. K., Subxankulov I., Imamnazarov D. H., Khomitov Sh. A.,** Nature of exchange interaction in amorphous alloys based on metals of iron group with metalloids, Metallofiz. Noveish. Tekhnol. 44 (7) (2022) 823–829.

27. **Moussa J. E., Schultz P. A., Chelikowsky J. R.,** Analysis of the Heyd – Scuseria – Ernzerhof density functional parameter space, J. Chem. Phys. 136 (20) (2012) 204117.

28. **Ribeiro R. A. P., Lazaro S. R., Pianaro S. A.,** Density functional theory applied to magnetic materials: Mn_3O_4 at different hybrid functionals, J. Magn. Magn. Mater. 391 (1 Oct) (2015) 166–171.

29. **Hirai S., Goto Y., Sakai Y., et al.,** The electronic structure of structurally strained Mn_3O_4 postspinel and the relationship with Mn_3O_4 spinel, J. Phys. Soc. Jpn. 84 (11) (2015) 114702.

30. **Larbi T., Doll K., Manoubi T.,** Density functional theory study of ferromagnetically and ferrimagnetically ordered spinel oxide Mn_3O_4. A quantum mechanical simulation of their IR and Raman spectra, J. Alloys Compd. 688-A (15 Dec) (2016) 692–698.

31. **Levämäki H., Vitos L.,** Electron localization function implementation in the exact muffin-tin orbitals method, Phys. Rev. B. 103 (3) (2021) 035118.

32. **James A. D. N., Harris-Lee E. I., Hampel A., et al.,** Wavefunctions, electronic localization and bonding properties for correlated materials beyond the Kohn – Sham formalism. arXiv preprint, Oct. 2020. [Online]. Available: https://arxiv.org/abs/2010.04694.

СПИСОК ЛИТЕРАТУРЫ

1. **Chen H., He J.** Facile synthesis of monodisperse manganese oxide nanostructures and their application in water treatment // The Journal of Physical Chemistry C. 2008. Vol. 112. No. 45. Pp. 17540–17545.

2. **Zhai Y., Zhai J., Zhou M., Dong S.** Ordered magnetic core–manganese oxide shell nanostructures and their application in water treatment // Journal of Materials Chemistry. 2009. Vol. 19. No. 38. Pp. 7030–7035.

3. **Chen H., Chu P. K., He J., Hu T., Yang M.** Porous magnetic manganese oxide nanostructures: synthesis and their application in water treatment // Journal of Colloid and Interface Science. 2011. Vol. 359. No. 1. Pp. 68–74.

4. **Imboon T., Khumphon J., Yotkuna K., Tang I-M., Sirikanjana Thongmee S.** Enhancement of photocatalytic by Mn_3O_4 spinel ferrite decorated graphene oxide nanocomposites // SN Applied Sciences. 2021. Vol. 3. 22 May. P. 653.

5. **Grundy A. N., Hallstedt B., Gauckler L. J.** Assessment of the Mn–O system // Journal of Phase Equilibria. 2003. Vol. 24. No. 1. Pp. 21–39.

6. **Safarov R. Z., Baikenov Y. A., Zhandildenova A. K., et al.** Phase transitions and structural evolution of manganese ores during high-temperature treatment // Metals. 2025. Vol. 15. No. 1. P. 89.

7. **Aminoff G.** Über die Kristallstruktur von Hausmannit ($MnMn_2O_4$) [On the crystal structure of hausmannite ($MnMn_2O_4$)] // Zeitschrift für Kristallographie – Crystalline Materials. 1926. Vol. 64. No. 1. Pp. 475–490.

8. **Jarosch D.** Crystal structure refinement and reflectance measurements of hausmannite, Mn_3O_4 // Mineralogy and Petrology. 1987. Vol. 37. No. 1. Pp. 15–23.

9. **Baron V., Gutzmer J., Rundlöf H., Tellgren R.** The influence of iron substitution on the magnetic properties of Hausmannite, $Mn^{2+}(Fe,Mn)^{3+}{}_2O_4$ // American Mineralogist. 1998. Vol. 83. No. 7–8. Pp. 786–793.

10. **Hosny N. M., Dahshan A.** Facile synthesis and optical band gap calculation of Mn_3O_4 nanoparticles // Materials Chemistry and Physics. 2012. Vol. 137. No. 2. Pp. 637–643.

11. **Dubal D. P., Dhawale D. S., Salunkhe R. R., Fulari V. J., Lokhande C. D.** Chemical synthesis and characterization of Mn_3O_4 thin films for supercapacitor application // Journal of Alloys and Compounds. 2010. Vol. 497. No. 1–2. Pp. 166–170.

12. **Jha A., Thapa R., Chattopadhyay K. K.** Structural transformation from Mn_3O_4 nanorods to nanoparticles and band gap tuning via Zn doping // Materials Research Bulletin. 2012. Vol. 47. No. 3. Pp. 813–819.

13. **Freitas E. T. F., Montoro L. A., Gasparon M., Ciminelli V. S. T.** Natural attenuation of arsenic in the environment by immobilization in nanostructured hematite // Chemosphere. 2015. Vol. 138. November. Pp. 340–347.

14. **Pulleri J. K., Singh S. K., Yearwar D., Saravanan G., Al-Fatesh A. S., Labhasetwar N. K.** Morphology dependent catalytic activity of Mn_3O_4 for complete oxidation of toluene and carbon monoxide // Catalysis Letters. 2020. Vol. 151. No. 1. Pp. 172–183.

15. **Gonçalves P. R. G., De Abreu H. A., Duarte H. A.** Stability, structural, and electronic properties of hausmannite (Mn_3O_4) surfaces and their interaction with water // The Journal of Physical Chemistry C. 2018. Vol. 122. No. 36. Pp. 20841–20849.

16. **Giannozzi P., Baroni S., Bonini N., et al.** QUANTUM ESPRESSO: a modular and open-source software project for quantum simulations of materials // Journal of Physics: Condensed Matter. 2009. Vol. 21. No. 39. P. 395502.

17. **Давлетшина А. Д., Якшибаев Р. А., Биккулова Н. Н.** Зонная структура твердых растворов халькогенидов меди и серебра // Научно-технические ведомости СПбГПУ. Физико-математические науки. 2013. № 2 (170). С. 33–38.

18. **Kuvandikov O. K., Shodiev Z. M., Khasanov Kh. B., Khairullaev B. A., Akhtamov J. Sh.** Ferrimagnetic properties of the $FeCr_2O_4$ chromite and $TiFe_2O_4$ titanomagnetite minerals at high temperatures // Metallofizika, Noveishie Tekhnologii. 2025. T. 47. № 6. C. 595–600.

19. **Kuvandikov O., Shodiev Z., Usarov U., Khairullaev B., Akhtamov J.** Paramagnetic properties of the rock minerals pyrrhotite and pentlandite at high temperatures // AIP Conference Proceedings. 2025. Vol. 3304. No. 1. P. 020009.

20. **Persson K.** Lawrence Berkeley National Laboratory and US. Department of Energy. Office of Scientific and Technical Information. Materials data on Mn_3O_4 (SG:141) by Materials Project // Materials Project. 2014. URL: https://doi.org/10.17188/1183671.

21. **Robie R. A., Hemingway B. S.** Low-temperature molar heat capacities and entropies of MnO_2 (pyrolusite), Mn_3O_4 (hausmanite), and Mn_2O_3 (bixbyite) // The Journal of Chemical Thermodynamics. 1985. Vol. 17. No. 2. Pp. 165–181.

22. **Chhor K., Bocquet J. F., Pommier C., Chardon B.** Heat capacity and thermodynamic behaviour of Mn_3O_4 and $ZnMn_2O_4$ at low temperatures // The Journal of Chemical Thermodynamics. 1986. Vol. 18. No. 1. Pp. 89–99.

23. **Jacob K. T., Kumar A., Rajitha G., Waseda Y.** Thermodynamic data for Mn_3O_4, Mn_2O_3 and MnO_2 // High Temperature Materials and Processes. 2011. Vol. 30. No. 4. Pp. 459–472.

24. **Duan J., Huang M., Song M., Zhou W., Tan H.** Suppressing Jahn –Teller distortion in manganese oxides for high-performance aqueous zinc-ion batteries // Materials. 2025. Vol. 18. No. 12. P. 2817.

25. **Yu X., Qian K., Du L., Zhang J., Lu N., Miao Z., Li Y., Kobayashi H., Yan X., Li R.** A strong Jahn – Teller distortion in Mn_3O_4–MnO heterointerfaces for enhanced silver catalyzed formaldehyde reforming into hydrogen // Sustainable Energy & Fuels. 2022. Vol. 6. No. 12. Pp. 3068–3077.

26. **Kuvandikov O. K., Subxankulov I., Imamnazarov D. H., Khomitov Sh. A.** Nature of exchange interaction in amorphous alloys based on metals of iron group with metalloids // Metallofizika i Noveishie Tekhnologii. 2022. Vol. 44. No. 7. Pp. 823–829.

27. **Moussa J. E., Schultz P. A., Chelikowsky J. R.** Analysis of the Heyd – Scuseria – Ernzerhof density functional parameter space // The Journal of Chemical Physics. 2012. Vol. 136. No. 20. P. 204117.

28. **Ribeiro R. A. P., Lazaro S. R., Pianaro S. A.** Density functional theory applied to magnetic materials: Mn_3O_4 at different hybrid functionals // Journal of Magnetism and Magnetic Materials. 2015. Vol. 391. 1 October. Pp. 166–171.

29. **Hirai S., Goto Y., Sakai Y., Wakatsuki A., Kamihara Y., Matoba M.** The electronic structure of structurally strained Mn_3O_4 postspinel and the relationship with Mn_3O_4 spinel // Journal of the Physical Society of Japan. 2015. Vol. 84. No. 11. P. 114702.

30. **Larbi T., Doll K., Manoubi T.** Density functional theory study of ferromagnetically and ferrimagnetically ordered spinel oxide Mn_3O_4. A quantum mechanical simulation of their IR and Raman spectra // Journal of Alloys and Compounds. 2016. Vol. 688. Part A. 15 December. Pp. 692–698.

31. **Levämäki H., Vitos L.** Electron localization function implementation in the exact muffin-tin orbitals method // Physical Review B. 2021. Vol. 103. No. 3. P. 035118.

32. **James A. D. N., Harris-Lee E. I., Hampel A., Aichhorn M., Dugdale S. B.** Wavefunctions, electronic localization and bonding properties for correlated materials beyond the Kohn – Sham formalism. arXiv preprint, Oct. 2020. [Online]. Available: https://arxiv.org/abs/2010.04694

THE AUTHORS

KUVANDIKOV Oblakul K.
Samarkand State University
15 University Blvd, Samarkand, 100104, Republic of Uzbekistan
quvandikov@rambler.ru
ORCID: 0000-0001-8750-038X

SHODIEV Zokir M.
Samarkand State University
15 University Blvd, Samarkand, 100104, Republic of Uzbekistan
shodiyevzm@gmail.com
ORCID: 0009-0000-8607-813X

AKHTAMOV Jushkin Sh.
Samarkand State University
15 University Blvd, Samarkand, 100104, Republic of Uzbekistan
texnalogiya11@gmail.com
ORCID: 0009-0007-7082-9251

СВЕДЕНИЯ ОБ АВТОРАХ

КУВАНДИКОВ Облакул Кувандикович – *доктор физико-математических наук, профессор кафедры общей физики Самаркандского государственного университета имени Шарофа Рашидова, г. Самарканд, Республика Узбекистан.*
100104, Республика Узбекистан, г. Самарканд, Университетский бульвар, 15
quvandikov@rambler.ru
ORCID: 0000-0001-8750-038X

ШОДИЕВ Зокир Миртозаевич – *кандидат физико-математических наук, доцент кафедры общей физики Самаркандского государственного университета имени Шарофа Рашидова, г. Самарканд, Республика Узбекистан.*
100104, Республика Узбекистан, г. Самарканд, Университетский бульвар, 15
shodiyevzm@gmail.com
ORCID: 0009-0000-8607-813X

АХТАМОВ Жушкин Шодмонович – *докторант (PhD студент), кафедры общей физики Самаркандского государственного университета имени Шарофа Рашидова, г. Самарканд, Республика Узбекистан.*
100104, Республика Узбекистан, г. Самарканд, Университетский бульвар, 15
texnalogiya11@gmail.com
ORCID: 0009-0007-7082-9251

Received 12.08.2025. Approved after reviewing 17.10.2025. Accepted 17.10.2025.
Статья поступила в редакцию 12.08.2025. Одобрена после рецензирования 17.10.2025. Принята 17.10.2025.